SP-258—3

Experimental Evaluation of Noncircular Reinforced Concrete Columns Strengthened with CFRP

by S. Rocca, N. Galati, and A. Nanni

Synopsis: This paper presents the results of an experimental investigation on the axial behavior of medium and large scale Reinforced Concrete (RC) columns of circular and non-circular cross-sections strengthened with unidirectional Carbon Fiber Reinforced Polymer (CFRP) wraps. A test matrix was developed to investigate the effect of different variables, such as the geometry of the specimen cross-section (circular, square, and rectangular), the side aspect ratio, and the area aspect ratio. A total of 22 specimens were divided into six series of three specimens each and two series of two specimens each. The largest and smallest columns featured cross-sectional areas of 0.8 m^2 (9 ft^2) and 0.1 m^2 (1 ft^2), respectively. All the specimens were subjected to pure axial compressive loading. The experimental results are compared with available data on RC specimens with one minimum dimension of the cross-section of 300 mm (12 in.). This evaluation allowed confirming that among circular and non-circular specimens of the same cross-sectional area and FRP volumetric ratio, the level of confinement effectiveness decreases as the side aspect ratio increases. Additionally, size effect within specimens of circular cross-section does not appear to be significant; however, for the case of non-circular specimens, scatter and limitation of data-points does not allow at the present time to draw a definite conclusion. A new analytical method that allowed estimating the confining pressure in non-circular cross-sections from the transverse strains at the corners is proposed. The obtained confining pressures and experimental results from this study allowed calibrating a strength model, which was validated with the available experimental data in the literature. Finally, the predictions of this strength model were compared to the ones by the model of Lam and Teng yielding close agreement.

Keywords: confinement; ductility; FRP strengthening; noncircular columns; reinforced concrete

ACI member **Silvia Rocca** is a Design Engineer at Structural Group. She received her MSc and PhD in civil engineering at the University of Missouri-Rolla. She received her BSc in civil engineering at the University of Piura, Peru. Her research interests include analysis, design, and retrofitting of RC structures.

ACI member **Nestore Galati** is a Design Engineer at Structural Group. He received his PhD in civil engineering at the University of Lecce, Italy, where he also received his BSc in materials engineering. He received his MSc in engineering mechanics at the University of Missouri-Rolla. His research interests include retrofitting of masonry and upgrade and in-situ load testing of RC structures.

Antonio Nanni, FACI, is a Professor and Chair of the Department of Civil, Architectural, and Environmental Engineering at the University of Miami and Professor at the University of Naples – Federico II. He was the founding Chair of ACI Committee 440, Fiber Reinforced Polymer Reinforcement, and is the Chair of ACI Committee 437, Strength Evaluation of Existing Concrete Structures.

INTRODUCTION

Confinement of Reinforced Concrete (RC) columns by means of Fiber Reinforced Polymer (FRP) jackets is a technique being used with growing frequency to seek the increment of load carrying capacity and/or ductility of such compression members.

The confinement of non-circular columns is generally acknowledged to be less efficient than the confinement of circular columns, since in the latter case, the wrapping provides circumferentially uniform confining pressure to the radial expansion of the compression member. In non-circular columns, the confinement is concentrated at the corners rather than over the entire perimeter.

Extensive work in both the experimental and analytical areas has been conducted on small-scale plain concrete specimens of circular and non-circular cross-sections confined with FRP and subjected to pure axial compressive loading (Carey and Harries 2003; De Lorenzis and Tepfers 2003; Lam and Teng 2003a,b; Masia et al. 2004). Studies focused on RC columns of both circular and non-circular cross-sections of considerable size (minimum-dimension of 300 mm [12 in.]) have also been conducted (Demers and Neale 1994; Kestner et al. 1997; Wang and Restrepo 2001; Youssef 2003; Carey and Harries 2003; Matthys et al. 2005); however, this experimental research has been limited due to high cost and lack of high-capacity testing equipment. This situation has been the main reason for overlooking the following important effects on the element performance that have not been accounted for in most of the available models: (a) the size of the cross-sectional area; (b) the dimensional aspect ratio of the cross-sectional area; (c) the possible detrimental effect of longitudinal steel reinforcement instability; (d) the concrete dilation dependant on the volumetric ratio; (e) and the contribution of the internal transverse steel reinforcement. In spite of these obstacles, several models to predict strength enhancement and in some instances stress-strain behavior have been proposed (Wang and Restrepo 2001; Lam and Teng 2003b; Maalej et al. 2003) and have become the basis for design provisions.

RESEARCH SIGNIFICANCE

So far, the vast majority of tests on non-circular columns have been on small samples. However, the design methods based upon these tests may not be reliable in predicting the strength enhancement and ductility in terms of axial deformation that might be achieved for larger columns found in practice. A systematic experimental investigation of the effect of column size is presented herein. This research study is now limited to specimens under pure axial loading condition, and this is considered the first step to understand the confinement process. Future work should include the effect of flexure and shear in order to develop complete interaction diagrams.

This research is of practical relevance in that there are thousands of RC structures (bridges and buildings) having non-circular columns that due to increases in load demands, changes in use or additions, or code updates require rapid and efficient strengthening with minimum disruption to users. Wrapping non-circular columns with FRP has the potential to achieve increments in strength and ductility with ease of installation, provided that fundamental behavior is understood.

EXPERIMENTAL PROGRAM

Test Program

The test matrix (Table 1) was developed to investigate the influence the effects of mainly two variables: the side aspect ratio (h/b) and area aspect ratio $A_g/A_{g(C)}$) on the effectiveness of FRP confined RC columns of non-circular cross-sections. The test matrix was divided into two sub-matrices based on the laboratories where the experiments were carried out: CALTRANS Seismic Response Modification Device Testing Laboratory (SRMD) at the University of California San Diego (UCSD) with 18 specimens (six series of three specimens each: A, B, C, D, E, and F), and the Building and Fire Research Laboratory at the National Institute of Standards and Technology (NIST) with four specimens (two series of two specimens each: G and H). Table 1 presents the characteristics of the test units in the following order: specimens label, cross-section dimensions (diameter of the circular columns D or side dimensions of the non-circular columns b and h), side aspect-ratio (h/b), overall specimens height (H), area of the gross section (A_g), area aspect-ratio ($A_g/A_{g(C)}$) (where $A_{g(C)}$ is the gross area of series C specimens), ratio of the area of longitudinal steel reinforcement to the cross-sectional area of the member (ρ_g), yield strength of longitudinal steel reinforcement (f_y), FRP volumetric ratio (ρ_f), and average concrete compressive strength at the corresponding age of testing of each column (f'_c).

Series A, B, C, D, E, and F consists of three specimens each: one control unit (A1, B1, C1, D1, E1, and F1), one unit strengthened to achieve an increment of 30% of load carrying capacity featuring a full wrapping scheme (A2, B2, C2, D2, E2, and F2), and a third unit (B3, C3, and D3) whose thickness of FRP jacket matched the same number of plies used in specimen A2. Specimens A3, E3, and F3 were partially wrapped for a 30% increment of carrying capacity as well. Series G and H were composed of two test units each: one control unit (G1 and H1), and one strengthened unit (G2 and H2) to gain 30% of increase in axial capacity. A gap of about 13 mm (0.5 in) was left at the top and bottom ends of the columns to avoid axial compressive loading of the FRP jacket. The partially wrapped specimens featured strips of 133 mm (5.25 in.) wide and a pitch of 76 mm (8.25 in.). Further details on the construction and strengthening of the specimens can be found in Rocca et al. (2006).

The detailing (concrete cover, longitudinal and transverse internal reinforcement layout, size, spacing, and shape of ties) of all the specimens was designed according to conventional RC practice (ACI 318-02). All the specimens featured a clear concrete cover of 38 mm (1.5 in.). The non-circular specimens were designed with a corner radius of 30 mm (1.2 in.). To prevent premature failure of the specimens at the top and bottom ends, steel transverse reinforcement spaced at about 50 mm (2 in.) was placed at these locations in all the specimens (Figure 1).

Material Properties

Concrete -- For the entire test program a nominal concrete compressive strength of 28 MPa (4,000 psi) representing the common strength in current building structures was considered appropriate. Since the specimens were cast at two different locations, the concrete constituents and properties are discussed separately.

All of the specimens at UCSD were built up from one single batch of ready-mix concrete having constituents and mix proportions as shown in Table 2. Standard concrete cylinders 152×305 mm (6×12 in.) were prepared and cured under the same conditions of the columns. These cylinders were tested according to ASTM C39-04 at 7, 14, 21, 28 days, and at the corresponding age at which the related columns were tested (three cylinders per each case). The average compressive strength for the characteristic ages were 20.1 MPa (2.92 ksi), 23.7 MPa (3.44 ksi), 26.3 MPa (3.81 ksi), and 30.5 MPa (4.43 ksi), respectively.

The constituents and mix proportions of the concrete for the specimens at NIST are presented in Table 3. Standard concrete cylinders were cast and tested at 7, 28 days and at the time of the actual testing of the columns. Due to the high congestion of the steel reinforcement at the top and bottom ends of the larger specimens (series G and H), a minimum slump of 20 cm (8 in.) was considered appropriate for the concrete to flow through the steel grids.

Reinforcing Steel -- Both UCSD and NIST specimens were designed with a Grade 60 (420 MPa) longitudinal steel reinforcement at a ratio of approximately 1.5%, Table 1 shows the average yielding strength of the steel used in

each of the specimens. These average values were obtained from tensile tests on coupons performed according to ASTM A370.

CFRP -- Unidirectional CFRP of one-ply nominal thickness (t_f) of 0.167 mm (0.0067 in.) was the wrapping material used for the entire research project. For the preliminary design, the mechanical properties provided by the manufacturer were used. One and two-plies tensile coupon tests were performed to determine the mechanical properties of the CFRP material used in the evaluation of the test results (ASTM D3039-00). The characterization yielded an ultimate tensile strain ε_{fu} of 0.93%, an ultimate tensile strength f_{fu} of 2668 MPa (387 ksi), and a modulus of elasticity E_f of 291 GPa (42,200 ksi).

Instrumentation and Test Set-up

The instrumentation consisted of electrical strain gauges located on the longitudinal and transverse steel reinforcement, and on the FRP jacket at critical locations (corner areas and mid-distance on each side) along the perimeter of the cross-section on the central region of the strengthened specimens. Additionally, external sensors to measure axial deformation (linear potentiometers in UCSD specimens and LVDTs in NIST specimens) were fixed to the faces of the columns at about mid-height.

The equipment at both UCSD and NIST laboratories is capable of applying an axial compressive force of 53 MN (12,000 kip). However, because of the height limitation of the one at UCSD (1.5 m [5 ft]), the larger specimens (groups G and H) were tested at NIST. The loading was quasi-static and it was applied in cycles of increments of one fifth of the expected capacity of each specimen. The minimum load level during unloading corresponded to approximately 5% of the total expected capacity. See Figures 2 and 3 for illustrations on the test set-ups at UCSD and NIST laboratories, respectively.

TEST RESULTS

The test results of the columns are shown in Table 4. The table shows the maximum load for the unconfined case (P_{co}) or the increase in axial compressive loading (P_{cc}/P_{co}), the concrete compressive strength corresponding to the maximum load for the unconfined case (f'_{co}) or the strengthening ratio (f'_{cc}/f'_{co}), the compressive strength of concrete at ultimate (f_{cu}), the axial compressive strain at maximum load (ε'_c and ε'_{cc} for the case of unconfined and confined, respectively), the axial compressive strain at ultimate (ε_{cu} and ε_{ccu} for the case of unconfined and confined members, respectively), the ratio of ultimate axial strain of confined member to unconfined ($\varepsilon_{ccu}/\varepsilon_{cu}$), and the average transverse strain on the FRP jacket at ultimate (ε_{tu}). The axial strains are the average values obtained from linear potentiometers of LVDTs fixed to the sides of the columns. The transverse strain for the circular specimens corresponds to the average value of the measurements obtained by the sensors on the jacket. For the case of the non-circular specimens, it is the mean value of the readings given by the sensors closer to the corners.

The experimental values of f_{cu} and ε_{ccu} (or ε_{cu} for the unconfined case) were reported according to the following definition: ε_{cu} is the ultimate strain of the unconfined RC column corresponding to $0.85f'_c$ (See curve a - Figure 4). For the confined RC column, ε_{ccu} may correspond to one of the following values: a) $0.85f'_{cc}$ in the case of a lightly confined member (See curve b - Figure 4); b) the failure strain in the heavily confined, softening case when the failure stress is larger than $0.85f'_{cc}$ (See curve c - Figure 4); or the heavily confined, hardening case, where ultimate strength corresponds to ultimate strain (See curve d - Figure 4). The definition of ε_{ccu} (or ε_{cu} for the unconfined case) at 85% of f'_{cc} (or f'_c for the unconfined case) is arbitrary for cases corresponding to curves a and b, although consistent with modeling of conventional concrete (Hognestad 1951), and such that the descending branch of the stress-strain curve at that level of stress ($0.85f'_{cc}$ or higher) is not as sensitive to the test procedure in terms of rate of loading and stiffness of the equipment utilized (Rocca et al. 2007).

In Table 4, strain values from specimen H1 are not reported due to an inconvenience with the Data Acquisition System in the last load cycle applied to this specimen. Additionally, the values of transverse strain on the FRP jacket of specimens F2 and H2 seemed to be inaccurate, and therefore are not reported either.

The failure mode of the confined columns was characterized by rupture of the FRP jacket in the central region of the member. This was generally followed by buckling of the longitudinal steel reinforcement. In the case of the non-circular specimens, the FRP rupture took place at the corners of the section. See Figure 5 for illustrations.

For the specimens of non-circular cross-section the increment of axial compressive capacity (P_{cc} /P_{co}) is marginal compared to that of the circular counterparts. However, in Table 4, performance of specimens in series E appears to be an exception. This series featured the same characteristics as series F (material and geometrical) with the sole difference being the overall specimen height: 0.7 m (2.3 ft) and 1.4 m (4.6 ft), in the case of series E and series F, respectively. The observed higher ratios of P_{cc} /P_{co} of series E compared to the ones from series F may be due to the unexpected premature failure of control unit E1. The possible cause maybe the limited number of ties that was able to be placed along the height of the specimen. Additionally, stress concentrations induced at the top and bottom ends might have affected the overall strength as well. For these reasons, the experimental results of specimens in series E are believed to be not truly representative and therefore are not included in the analysis.

ANALYSIS AND DISCUSSION OF RESULTS

Figures 6(a), (b), and (c) present the performance of the specimens in terms of the ratio f'_{cc}/f'_{co}, which is a measurement of the confinement effectiveness, and the variables: side aspect ratio and area aspect ratio. In these figures, the label numbers within brackets represent the FRP volumetric ratio in percentages. Figure 6(a) shows the influence of the cross-sectional shape in the strengthening performance of specimens of a constant cross-sectional area ($A_g/A_{g(C)} = 1$). It can be observed that among specimens of different cross-sectional shape featuring similar FRP volumetric ratio (ρ_f), and taking the circular specimens with a ratio h/b equal to zero as a "benchmark", the level of confinement effectiveness decreases as the side aspect ratio increases. Figure 6(b) and Figure 6(c) show the effect of the area aspect ratio for specimens of square and rectangular cross-sections, respectively. In these two figures, there seems to be decreasing confinement effectiveness trend as the area-aspect ratio increases, however, a definite conclusion cannot be drawn due to the limited amount of data available.

The results from this experimental program are also presented along with collected available data on RC columns of circular and non-circular cross-sections with one minimum dimension of the cross-section of 300 mm (12 in.), side aspect ratios not greater than 2, and FRP jackets with the fibers oriented perpendicular to the longitudinal axis of the column. The collected data on circular and non-circular RC specimens is shown in Table 5 and Table 6, respectively. Table 5 is composed of a total of 20 specimens divided in five sets of experiments, and Table 6 presents 13 specimens divided in six experimental sets. The specimens' codes correspond to the studies conducted by the following authors: "DN" to Demers and Neale (1994), "KE" to Kestner et al. (1997), "YO" to Youssef (2003), "CH" to Carey and Harries (2003), "MA" to Matthys et al. (2005), and "WR" to Wang and Restrepo (2001). Circular specimens "YO" were divided in two groups depending on the type of transverse steel reinforcement, that is: "-s" for spiral and "-h" for hoops. In Table 5 and Table 6, the data is presented in terms of the following parameters: type of FRP used, diameter of the circular cross-sections (D); side dimensions (b, h) and the chamfered corner radius of the non-circular specimens (r); overall height (H); longitudinal and transverse steel reinforcement ratio (ρ_g and ρ_t); FRP volumetric ratio (ρ_f); unconfined concrete compressive strength (f'_c); yield strength of the longitudinal and transverse steel reinforcement (f_y and f_{yt}); FRP mechanical properties (E_f, f_{fu}, and ε_{fu}); nominal ply thickness of FRP (t_f); maximum loads for the unconfined cases (P_{co}) or the increase in axial compressive loading (P_{cc}/P_{co}); and concrete compressive strengths corresponding to the maximum load for the unconfined cases (f'_{co}) or the strengthening ratio (f'_{cc}/f'_{co}).

All the experimental data is presented in Figure 7 in terms of trends of the strengthening ratio f'_{cc}/f'_{co} versus the parameter $\rho_f E_f/E_c$, which represents the ratio of the stiffness of the FRP jacket to the axial stiffness of the concrete. The product of the parameters ρ_f and E_f resembles the theoretical stiffness of the FRP jacket (E_j), also known as confinement modulus or lateral modulus (Xiao and Wu 2000; De Lorenzis and Tepfers 2001). This parameter represents the capacity of the FRP jacket of restraining the lateral dilation of the concrete. In the case of circular specimens, E_j is directly related to the maximum confining pressure as follows:

$$f_{l,f} = \left(\frac{2nt_f E_f}{D}\right)\varepsilon_{fu} = \left(\frac{1}{2}\rho_f E_f\right)\varepsilon_{fu} = \left(E_j\right)\varepsilon_{fu} \qquad (1)$$

However, in the case of non-circular specimens, E_j depends on the definition given to determine the equivalent confining pressure $f_{l,f}$, which in most of the cases is multiplied by a shape factor. Different authors have suggested varied expressions for this shape factor along with their applicability limitations being mainly the side-aspect ratio (h/b) and maximum side dimension. These expressions depend on the geometry of the cross-section, chamfered corner radius, and longitudinal steel reinforcement ratio (Lam and Teng 2003b; Rocca et al. 2007). Since for non-circular cross-sections a definite expression for $f_{l,f}$ has not been yet established, and consequently for the lateral modulus E_j, it was considered appropriate to present the collected data and experimental results using the parameters ρ_f and E_f. Additionally, the use of the concrete modulus E_c was included to reflect the variation of concrete compressive strengths (f'_c) among the different tests.

Figures 7(a), (b), (c) refer to cases of specimens of circular, square and rectangular cross-sections, respectively. Figure 7(d) presents the linear trends of the types of cross-sections and their reliability indexes obtained by regression analysis corresponding to each data-set. In the legends, each specimen acronym is followed by a number(s) that indicate the dimensions of the cross-section (D, b, h).

Note the uniformity of the trend and minor scattering of the circular cross-section data-set in Figure 7(a). No pattern reflecting the effect of cross-sectional area size is identified leading to the establishment of the lack of such effect on this type of cross-section. In Figure 7(b), the square cross-section data-set, the scatter of data is more pronounced. In Figure 7(c), the specimens of rectangular cross-sections, no definite observation can be concluded due to the high level of data scattering and the limited number of data points. The linear trends of the three data-sets presented in Figure 7(d) reflect the level of effectiveness of the FRP confinement in the axial strengthening. The slopes of the trends corresponding to the non-circular specimens reflect their strengthening performance being less effective than in the case of specimens of circular cross-sections, which confirms the generally accepted notion of confinement of different cross-section shapes.

PROPOSED ANALYTICAL MODEL

It is widely acknowledged that in a FRP wrapped column of non-circular cross-section, the effectively confined concrete area is defined by four second-degree parabolas (Figure 8). The current approach to determine the confining pressure for this type of cross-section consists in defining an equivalent circular section having a reduced efficiency identified by the shape factor that accounts for the geometry of the section. The diameter of this equivalent circular section varies according to different authors, such as: the smallest side dimension (Mirmiran et al. 1998), the diagonal of the non-circular cross-section (Lam and Teng 2003b).

Transverse or hoop strains measured in a circular cross-section can be directly used to compute the total acting confining pressure "f_l", however, in the case of a non-circular section, measured strains along the perimeter cannot be directly correlated to "f_l" (Harries and Carey 2002). A proposed idealization of this problem is presented in what follows.

The relation between "f_l" and the transverse strain in the FRP and steel reinforcement may be obtained by idealizing a portion of the concrete confined area as a two-hinged parabolic symmetrical arch restrained by an horizontal tie representing FRP and transverse steel reinforcement, and subjected to a uniformly distributed load representing the confining pressure (Figure 9). For the analysis, the following assumptions/simplifications were considered: (a) the intersection of the parabola with the edges of the section is 45° (Lam and Teng 2003b); (b) the span "L" of the arch coincides with the side of the cross-section; (c) the thickness of the arch is constant and equal to twice the chamfered corner radius; and (d) the loading span is equal to the side of the cross-section. The total internal force in the horizontal tie of the arch is equal to $T_f + T_s$, where "T_f" is the FRP tensile force and "T_s" is the steel tensile force. In a longitudinal portion of the column of height equal to the transverse steel reinforcement pitch "s", "T_f" and "T_s" can be computed with Eqs. (2) and (3) (Fertis 1996):

$$T_f = E_f \varepsilon_f n t_f s \tag{2}$$

$$T_s = A_s E_s \varepsilon_s \tag{3}$$

The confining pressures due to the steel reinforcement and FRP can be obtained by solving the structure defined in Figure 9 based on equilibrium and the theorem of Castigliano (Fertis 1996), leading to the following expressions:

$$f_{l,f} = 8\,T_f h_a / L^2 \quad (4)$$

$$f_{l,s} = 8\,T_s h_a / L^2 \quad (5)$$

Where, "h_a" is the height of the parabolic arch at its centerline. The rest of the parameters in the equations above have been previously defined in the text. For the derivation of Equations (4) and (5) please refer to Rocca (2007).

In the presented experimental program, transverse strains on the steel and FRP were recorded at locations close to the corners of the specimens (approximately at the change of curvature). These strains were used to estimate the values of "T_f", "T_s", and the corresponding confining pressures ($f_{l,f}$ and $f_{l,s}$). With the values of "$f_{l,f}$" and "$f_{l,s}$", and the concrete compressive strength of the confined and unconfined concrete (f'_{cc} and f'_{co}), two efficiency factors "k" were calibrated following the empirical formula proposed by Richart et al. (1928):

$$f'_{cc} / f'_{co} = 1 + k\, f_l / f'_{co} \quad (6)$$

Two cases were considered to observe the possible contribution of the internal transverse steel reinforcement to the confinement. For the first case, the total acting confining pressure "f_l" is composed by two terms reflecting both the contribution of the FRP jacket and the contribution of the steel transverse reinforcement, that is: $f_l = f_{l,f} + f_{l,s} \cdot A_{cc}/A_g$. For the second case, "$f_l$" only accounts for the pressure induced by the FRP jacket, that is: $f_l = f_{l,f}$. Values of f'_{cc}/f'_{co} versus the ratio f_l/f'_{co} corresponding to the non-circular specimens of the presented experimental program are plotted in Figure 10. Both sets of data-points show very similar ratios f_l/f'_{co} which indicate that the contribution of the transverse steel reinforcement to the confinement pressure is minimal and therefore may be neglected. Then, the estimated value of k = 0.61 with a reliability index of 0.77 resulting from a regression analysis and corresponding to the second case is used to evaluate this strength model.

The performance of this proposed model to estimate the confining pressure in a non-circular section and therefore the increment of concrete compressive strength (f'_{cc}/f'_{co}) is evaluated using the experimental results from this study and available collected data presented in Tables 3 and 4. Additionally, these predictions are compared to those given by the model of Lam and Teng (2003b), since this experimental model was calibrated with an extensive database of small plain concrete prisms and it has shown to yield acceptable predictions when estimating the capacity of RC confined columns (Rocca et al. 2008).

Figure 11 shows the theoretical versus experimental ratios of f'_{cc}/f'_{co}. The 45° line corresponds to a perfect agreement between predictions and experiments. The points falling above this line represent overestimations of the experimental values. An average absolute error, standard deviation, and coefficient of variation of 4.79%, 2.46%, and 51% showed that the proposed model performed well in predicting the experimental results. The close agreement between both models constitutes a verification of the proposed analytical method to correlate the measured transverse strains (on steel reinforcement and FRP) to the confining pressure and compute the increment of compressive strength.

SUMMARY AND CONCLUSIONS

The paper presents the experimental performance under axial load of FRP-confined RC columns of circular and non-circular cross-sections with minimum and maximum cross-sectional areas of 0.1 m^2 (1 ft^2) and 0.8 m^2 (9 ft^2), respectively. A test matrix composed of a total of 22 RC columns divided into six series of three specimens each and two series of two specimens each, was developed to study the effects of variable cross-sectional area, shape (circular, square, and rectangular), and side aspect ratio. These specimens were tested under pure axial loading condition as the first step to understand the confinement process to be later considered within the effects of combined axial force and bending moment to develop practical design interaction diagrams.

The results obtained in this experimental program were compared to RC columns of relevant size available in the literature. The performance of the specimens was compared based on the strengthening ratio f'_{cc}/f'_{co}, and the variables of side-aspect ratio and area-aspect ratio for square and rectangular specimens. Additionally, a proposed

new analytical method to correlate the transverse strains on steel and FRP to the confining pressures was evaluated. The following conclusions can be made from this study:

- Even though the increments of compressive strength in the non-circular specimens was not significant, test units B2, C2, E3, F2, F3, and G2, did exhibit ductility in terms of axial deformation. The highest level of increment of compressive strength and ductility were observed in specimen B2 (wrapped with seven plies) with 24% and 905%, respectively;
- The level of confinement effectiveness for specimens of different cross-sectional shape featuring the same cross-sectional area size and similar FRP volumetric ratio, decreases as the side-aspect ratio increases;
- Specimens of circular cross-section showed the highest level of confinement effectiveness in axial strengthening. No pattern reflecting the effect of the size of the cross-section is identified leading to believe on the lack of such effect on this type of cross-section;
- For the case of non-circular specimens, few indicatives of the possible negative effect of cross-sectional area size in the axial strengthening were noted, however, the scattering and limitation of data-points do not allow at the present time to draw a definite conclusion;
- Since in the non-circular specimens, the transverse strains measured along the perimeter cannot be directly related to the confinement pressure "f_l", a new analytical approach was proposed to determine "f_l" using the strains close to the corners of the section. This method consists of idealizing a portion of the concrete confined area as a two-hinged parabolic arch restrained by a horizontal tie representing FRP and transverse steel reinforcement, and subjected to a uniformly distributed load. With the obtained values of confining pressures it was possible to calibrate a strength model and evaluate it with the collected experimental data. Additionally, the performance of this strength model was compared to the one by Lam and Teng showing close agreement in the predictions;
- The contribution of the transverse steel reinforcement to the confining pressure in the specimens of this experimental program computed using the proposed analytical model was found to be negligible;
- Since the proposed analytical method and strength model were calibrated with the experimental data from the present study, and was validated with limited experimental data available in the literature, further experimental evidence is needed to confirm the validity of the model.

ACKNOWLEDGEMENTS

The authors would like to acknowledge the funding and support received from: National Science Foundation (supplement grant number 0453808), MAPEI S.p.A. in Milan (Italy) for donating the FRP material, NSF Industry/University Cooperative Research Center on Repair of Buildings and Bridges with Composites (RB2C).

A special recognition is given to Dr. Nicholas Carino and Mr. Frank Davis at NIST, and Dr. Gianmario Benzoni and Mr. Donato Innamorato at UCSD, for their cooperation conducting the tests.

LIST OF NOTATIONS

The following symbols are used in this paper:

A_g	Area of the gross section, mm^2
$A_{g(C)}$	Area of the gross section of specimens series C = 457×457 mm
$A_g/A_{g(C)}$	Area aspect-ratio or ratio of a given gross area section to the gross area section of series C specimens
A_s	Area of steel reinforcement, mm^2
b	Short side dimension of a non-circular cross-section, mm
b_f	Width of FRP jacket strip in partial wrapping, mm
D	Diameter of circular cross-section, mm
E_c	Initial modulus of elasticity of concrete, MPa
E_f	Tensile modulus of elasticity of FRP, MPa
f'_c	Concrete compressive strength determined from standard cylinder, MPa
f'_{co}	Maximum compressive strength of unconfined concrete, MPa
f'_{cc}	Maximum compressive strength of confined concrete, MPa
f_{cu}	Ultimate compressive strength of concrete, MPa
f_{fu}	Ultimate tensile strength of FRP, MPa

f_y Yield strength of longitudinal steel reinforcement, MPa
H Height of column, m
h Long side dimension of a non-circular cross-section, mm
h/b Side aspect-ratio or ratio of the long side dimension to the short one in a non-circular section
n Number of FRP plies composing the jacket
P_{co} Maximum axial compressive load of unconfined column, kN
P_{cc} Maximum axial compressive load of confined column, kN
s Pitch of FRP jacket in partial wrapping, mm
t_f FRP nominal ply thickness, mm

ε'_c Axial compressive strain at maximum load of unconfined column, mm/mm
ε'_{cc} Axial compressive strain at maximum load of confined column, mm/mm
ε_{ccu} Ultimate axial compressive strain of confined concrete, mm/mm
ε_{cu} Ultimate axial compressive strain of unconfined concrete, mm/mm
ε_{fu} Ultimate tensile strain of the FRP, mm/mm
ε_{tu} Average tensile strain of the FRP at ultimate, mm/mm

ρ_f Volumetric ratio of FRP reinforcement = $\begin{cases} \left(4nt_f/D\right)\left(b_f/s\right) & \text{Circular} \\ \left(2nt_f\left(b+h\right)/bh\right)\left(b_f/s\right) & \text{Non-Circular} \end{cases}$

ρ_g Ratio of the area of longitudinal steel reinforcement to the cross-sectional area of a compression member = A_s/A_g

REFERENCES

ACI 318, 2002, "Building Code Requirements for Structural Concrete and Commentary," American Concrete Institute, Farmington Hills, MI, USA.

ASTM., 2000, "Standard Test Method for Tensile Properties of Polymer Matrix Composite Materials," ASTM D 3039, West Conshohocken, PA.

ASTM., 2003, "Standard Test Methods and Definitions for Mechanical Testing of Steel Products," ASTM A 370, West Conshohocken, PA.

ASTM., 2004, "Standard Test Method for Compressive Strength of Cylindrical Concrete Specimens," ASTM C 39, West Conshohocken, PA.

Carey, S.; and Harries, K., 2003, "The Effects of Shape, 'Gap', and Scale on the Behavior and Modeling of Variably Confined Concrete," *Report No. ST03-05*, University of South Carolina, Columbia, SC.

De Lorenzis, L.; and Tepfers, R., 2003, "Comparative Study of Models on Confinement of Concrete Cylinders with Fiber-Reinforced Polymer Composites," *ASCE Journal of Composites for Construction*, V. 7, No. 3, pp. 219-237.

Demers, M.; and Neale, K., 1999, "Confinement of Reinforced Concrete Columns with Fibre Reinforced Composites Sheets – An Experimental Study," *Canadian Journal of Civil Engineering*, No. 26, pp. 226-241

Hognestad, E., 1951, "A Study of Combined Bending and Axial Load in Reinforced Concrete Members," Bulletin 399, University of Illinois Engineering Experiment Station, Urbana, IL.

Kestner, J. T.; Harries, K. A.; Pessiki, S. P.; Sause, R.; and Ricles, J. M., 1997, "Rehabilitation of Reinforced Concrete Columns using Fiber Reinforced Polymer Composite Jackets," *ATLSS Report No. 97-07*, Lehigh University, Bethlehem, PA.

Lam, L.; and Teng, J.; 2003a, "Design-oriented Stress-Strain Model for FRP-confined Concrete," *Construction and Building Materials*, V. 17, pp. 471-489.

Lam, L., and Teng, J., 2003b, "Design-oriented Stress-Strain Model for FRP-confined Concrete in Rectangular Columns," *Journal of Reinforced Plastics and Composites*, V. 22, No. 13, pp. 1149-1186.

Maalej, M.; Tanwongsval, S.; and Paramasivam, P., 2003, "Modeling of Rectangular RC Columns Strengthened with FRP," *Cement & Concrete Composites*, V. 25, pp. 263-276.

Masia, M.; Gale, T.; Shrive, N., 2004, "Size Effects in Axially Loaded Square-Section Concrete Prisms Strengthened Using Carbon Fibre Reinforced Polymer Wrapping," *Canadian Journal of Civil Engineering*, V. 31, pp. 1-13.

Matthys, S.; Toutanji, H.; Audenaert, K.; and Taerwe, L., 2005, "Axial Load Behavior of Large-Scale Columns Confined with Fiber-Reinforced Polymer Composites," *ACI Structural Journal*, V. 102, No. 2, pp. 258-267.

Rocca, S.; Galati, N.; and Nanni, A., 2006, "Experimental Evaluation of FRP Strengthening of Large-Size Reinforced Concrete Columns," *CIES Report No. 06-63*, University of Missouri – Rolla, Rolla, MO.

Rocca, S. 2007, "Experimental and Analytical Evaluation of FRP-Confined Large Size Reinforced Concrete Columns," Ph. D. Dissertation, University of Missouri-Rolla, Rolla, MO, USA.

Rocca, S; Galati, N; and Nanni, A., 2008, "Review of International Design Guidelines for FRP Confinement of Reinforced Concrete Columns of Prismatic Cross-Section," *ASCE Journal of Composites for Construction*, V. 12, No. 1.

Wang, Y. C.; and Restrepo, J. I., 2001, "Investigation of Concentrically Loaded Reinforced Concrete Columns Confined with Glass Fiber-Reinforced Polymer Jackets," *ACI Structural Journal*, V. 98, No. 3, pp. 377-385.

Youssef, M.N., 2003, "Stress Strain Model for Concrete Confined by FRP Composites," Ph. D. Dissertation, University of California-Irvine, Irvine, CA, USA.

Table 1 -- Test Program

Test Unit	D or b × h (mm)	$\frac{h}{b}$	H (m)	A_g (cm^2)	$\frac{A_g}{A_{g(C)}}$	ρ_g (%)	f_y (MPa)	ρ_f (%)	f'_c (MPa)
A1	508	NA	1.1	2027	NA	1.53	446	0.00	31.7
A2								0.26	31.9
A3								0.33	31.9
B1	313 × 635	2.0	1.4	1984	1	1.56	447	0.00	30.2
B2								1.12	30.4
B3								0.32	30.4
C1	457 × 457	1.0	1.0	2090	1	1.48	446	0.00	32.1
C2								0.58	32.3
C3								0.29	32.1
D1	648 × 648	1.0	1.4	4195	2	1.48	446	0.00	30.7
D2								0.52	30.9
D3								0.21	30.7
E1	324 × 324	1.0	0.7	1049	0.5	1.53	447	0.00	32.3
E2								0.41	33.0
E3								0.53	33.2
F1	324 × 324	1.0	1.4	1049	0.5	1.53	447	0.00	31.5
F2								0.41	31.5
F3								0.53	31.7
G1	914 × 914	1.0	2.0	8361	4	1.50	690	0.00	31.6
G2								0.58	31.6
H1	635 × 1270	2.0	2.7	8065	4	1.52	690	0.00	30.3
H2								1.50	30.3

Note: 1 mm = 0.04 in.; 1 cm^2 = 0.155 $in.^2$; 1 MPa = 0.145 ksi; NA = Not Applicable.

Table 2 -- Concrete Mix Proportions; UCSD Specimens

Portland Cement Type I	284 kg/m^3 (478 lb/yd^3)
Fly Ash	53 kg/m^3 (90 lb/yd^3)
Coarse Gravel (12.5 mm [0.5 in])	682 kg/m^3 (1150 lb/yd^3)
Water	208 kg/m^3 (350 lb/yd^3)
Admixture WRDA-64	10 kg/m^3 (17 lb/yd^3)
Air-Entraining Agent	2%

Table 3 -- Concrete Mix Proportions; NIST Specimens

Portland Cement Type I-II	307 kg/m^3 (517 lb/yd^3)
Fine Aggregate	987 kg/m^3 (1664 lb/yd^3)
Coarse Aggregate (#8 gravel)	934 kg/m^3 (1575 lb/yd^3)
Water	148 kg/m^3 (250 lb/yd^3),
High-Range Water Reducer (HRWR)	0.77 kg/m^3 (1.29 lb/yd^3)

Table 4 -- Test Results

Test Unit	ρ_f (%)	P_{co} (kN) or $\left[\frac{P_{cc}}{P_{co}}\right]$	f'_{co} (MPa) or $\left[\frac{f'_{cc}}{f'_{co}}\right]$	f_{cu} (MPa)	ε'_c or ε'_{cc} (%)	ε_{cu} or ε_{ccu} (%)	$\frac{\varepsilon_{ccu}}{\varepsilon_{cu}}$	ε_{tu} (%)
A1	0.00	6643	26.35	26.35	0.26	0.26	1.00	NA
A2	0.26	[1.35]	[1.44]	37.97	1.23	1.23	4.72	0.85
A3	0.33	[1.39]	[1.49]	37.50	0.74	1.47	5.65	0.96
B1	0.00	5923	24.47	17.87	0.17	0.18	1.00	NA
B2	1.12	[1.26]	[1.24]	25.84	0.29	1.53	8.72	0.49
B3	0.32	[1.07]	[1.01]	21.12	0.23	0.54	3.07	0.08
C1	0.00	6741	26.01	23.33	0.24	0.24	1.00	NA
C2	0.58	[1.09]	[1.12]	26.62	0.47	1.10	4.52	0.58
C3	0.29	[1.05]	[1.06]	20.79	0.27	0.85	3.53	0.63
D1	0.00	13265	25.38	22.01	0.25	0.29	1.00	NA
D2	0.52	[1.16]	[1.20]	25.79	0.39	0.51	1.77	0.39
D3	0.21	[1.06]	[1.07]	23.17	0.31	0.42	1.46	0.37
E1	0.00	2673	21.17	18.33	0.15	0.15	1.00	NA
E2	0.41	[1.49]	[1.49]	27.02	0.23	0.31	2.05	0.65
E3	0.53	[1.54]	[1.56]	30.37	0.33	1.20	7.92	0.68
F1	0.00	3451	26.46	22.44	0.32	0.54	1.00	NA
F2	0.41	[1.11]	[1.14]	25.77	0.31	0.95	1.77	NR
F3	0.53	[1.11]	[1.14]	27.38	0.48	1.86	3.46	0.62
G1	0.00	28177	26.18	22.26	0.26	0.44	1.00	NA
G2	0.58	[1.10]	[1.05]	23.27	0.33	0.81	1.86	0.45
H1	0.00	27588	24.10	NR	NR	NR	NA	NA
H2	1.50	[1.13]	[1.19]	24.24	0.34	0.54	NA	NR

Note: 1 kN = 0.225 kip; 1 MPa = 0.145 ksi; NA = Not Applicable; NR = Not Reported.

Table 5 -- Experimental Data; Circular RC Specimens

Test Unit	FRP Type	D (mm)	H (m)	ρ_g (%)	ρ_t (%)	ρ_f (%)	f'_c (MPa)	f_y (MPa)	f_{yt} (MPa)	E_f (MPa)	f_{fu} (MPa)	ε_{fu} (%)	t_f (mm)	P_{co} (kN) or [P_{cc}/P_{co}]	f'_{co} (MPa) or [f'_{cc}/f'_{co}]
(1)	(2)	(3)	(4)	(5)	(6)	(7)	(8)	(9)	(10)	(11)	(12)	(13)	(14)	(15)	(16)
DN1	NA	300	1.2	1.40	0.63	0.00	25.0	400	400	NA	NA	NA	NA	1830	20.58
	CFRP	300	1.2	1.40	0.63	1.20	25.0	400	400	84002	1269	1.50	0.30	[1.41]	[1.52]
DN2	NA	300	1.2	3.50	1.26	0.00	25.0	400	400	NA	NA	NA	NA	2640	24.20
	CFRP	300	1.2	3.50	1.26	1.20	25.0	400	400	84002	1269	1.50	0.30	[1.38]	[1.61]
DN3	NA	300	1.2	1.40	1.26	0.00	40.0	400	400	NA	NA	NA	NA	3439	43.67
	CFRP	300	1.2	1.40	1.26	1.20	40.0	400	400	84002	1269	1.50	0.30	[1.24]	[1.28]
KE1	NA	508	1.8	1.53	0.19	0.00	31.5	457	501	NA	NA	NA	NA	7476	30.35
KE2	GFRP	508	1.8	1.53	0.19	2.04	31.5	457	501	25000	441	1.90	0.86	[1.21]	[1.26]
KE3	CFRP	508	1.8	1.53	0.19	0.39	31.5	457	501	230,909	3516	1.50	0.17	[1.51]	[1.62]
YO1 s	NA	406	0.8	1.50	0.21	0.00	47.1	414	276	NA	NA	NA	NA	5918	40.11
YO2 s	CFRP	406	0.8	1.50	0.21	2.30	47.1	414	276	103,839	1246	1.25	0.58	[1.83]	[1.96]
YO3 s	CFRP	406	0.8	1.50	0.21	2.30	47.1	414	276	103,839	1246	1.25	0.58	[1.66]	[1.76]
YO1 h	NA	406	0.8	1.50	0.21	0.00	38.4	414	276	NA	NA	NA	NA	4975	32.71
YO2 h	CFRP	406	0.8	1.50	0.21	2.30	38.4	414	276	103,839	1246	1.25	0.58	[2.03]	[2.22]
YO3 h	CFRP	406	0.8	1.50	0.21	2.30	38.4	414	276	103,839	1246	1.25	0.58	[1.79]	[1.94]
CH1	NA	610	1.8	1.40	0.33	0.00	33.5	414	441	NA	NA	NA	NA	13386	40.64
CH2	CFRP	610	1.8	1.40	0.33	1.97	33.5	414	441	72500	883	1.21	1.00	[1.59]	[1.68]
MA1	NA	400	2.0	0.90	0.37	0.00	36.1	620	560	NA	NA	NA	NA	4685	32.53
MA2	CFRP	400	2.0	0.90	0.37	0.59	36.1	620	560	198,000	2600	1.19	0.12	[1.59]	[1.67]
MA4	GFRP	400	2.0	0.90	0.37	1.80	36.1	620	560	60000	780	1.30	0.30	[1.62]	[1.70]
MA5	GFRP	400	2.0	0.90	0.37	0.60	36.1	620	560	60000	780	1.30	0.30	[1.14]	[1.14]
MA6	GFRP	400	2.0	0.90	0.37	0.60	36.1	620	560	60000	780	1.30	0.30	[1.07]	[1.06]
MA8	HFRP	400	2.0	0.90	0.37	0.49	36.1	620	560	120,000	1100	0.96	0.12	[1.33]	[1.36]

Note: 1 mm = 0.04 in.; 1 MPa = 0.145 ksi; 1 kN = 0.225 kip; NA = Not Applicable.

Table 6 -- Experimental Data; Non-Circular RC Specimens

Test Unit	Type	b (mm)	h (mm)	h/b	H (m)	r (mm)	ρ_g (%)	ρ_t (%)	ρ_f (%)	f'_c (MPa)	f_y (MPa)	f_{yt} (MPa)	E_f (MPa)	f_{fu} (MPa)	ε_{fu} (%)	t_f (mm)	P_{co} (kN) or $[P_{cc}/P_{co}]$	f'_{co} (MPa) or $[f'_{cc}/f'_{co}]$
(1)	(2)	(3)	(4)	(5)	(6)	(7)	(8)	(9)	(10)	(11)	(12)	(13)	(14)	(15)	(16)	(17)	(18)	(19)
KE1	NA	457	457	1.0	1.8	38	1.48	0.11	0.00	31.5	457	502	NA	NA	NA	NA	7340	28.81
KE3	GFRP	457	457	1.0	1.8	38	1.48	0.11	2.27	31.5	457	502	25000	443	1.90	0.86	[1.13]	[1.16]
KE4	CFRP	457	457	1.0	1.8	38	1.48	0.11	0.43	31.5	457	502	230,909	3515	1.50	0.17	[1.19]	[1.23]
WR1	NA	300	300	1.0	0.9	30	1.50	0.62	0.00	18.9	439	365	NA	NA	NA	NA	2127	17.31
WR2	GFRP	300	300	1.0	0.9	30	1.50	0.62	3.39	18.9	439	365	20500	375	2.00	1.27	[1.19]	[1.26]
WR3	NA	300	450	1.5	0.9	30	1.50	0.62	0.00	18.9	439	365	NA	NA	NA	NA	3268	17.89
WR4	GFRP	300	450	1.5	0.9	30	1.50	0.62	2.82	18.9	439	365	20500	375	2.00	1.27	[1.10]	[1.14]
YO1	NA	381	381	1.0	0.8	38	1.60	0.55	0.00	41.2	414	276	NA	NA	NA	NA	5967	35.05
YO2	CFRP	381	381	1.0	0.8	38	1.60	0.55	2.45	41.2	414	276	103,839	1246	1.25	0.58	[1.25]	[1.29]
YO3	NA	254	381	1.5	0.8	38	1.60	0.74	0.00	41.1	414	276	NA	NA	NA	NA	3966	34.92
YO4	CFRP	254	381	1.5	0.8	38	1.60	0.74	3.07	41.1	414	276	103,839	1246	1.25	0.58	[1.11]	[1.13]
CH1	NA	540	540	1.0	1.6	51	1.10	0.41	0.00	33.5	414	441	NA	NA	NA	NA	14196	43.46
CH2	CFRP	540	540	1.0	1.6	51	1.10	0.41	2.22	33.5	414	441	72500	875	1.21	1.00	[1.04]	[1.04]

Note: 1 mm = 0.04 in.; 1 MPa = 0.145 ksi; 1 kN = 0.225 kip; NA = Not Applicable.

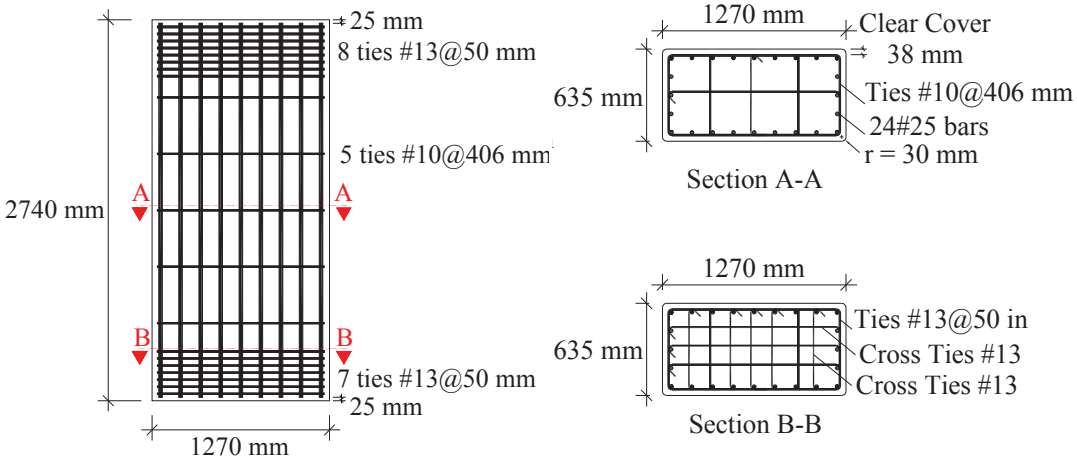

Figure 1 -- Schematic of Reinforcement Layout - Specimens Series H.

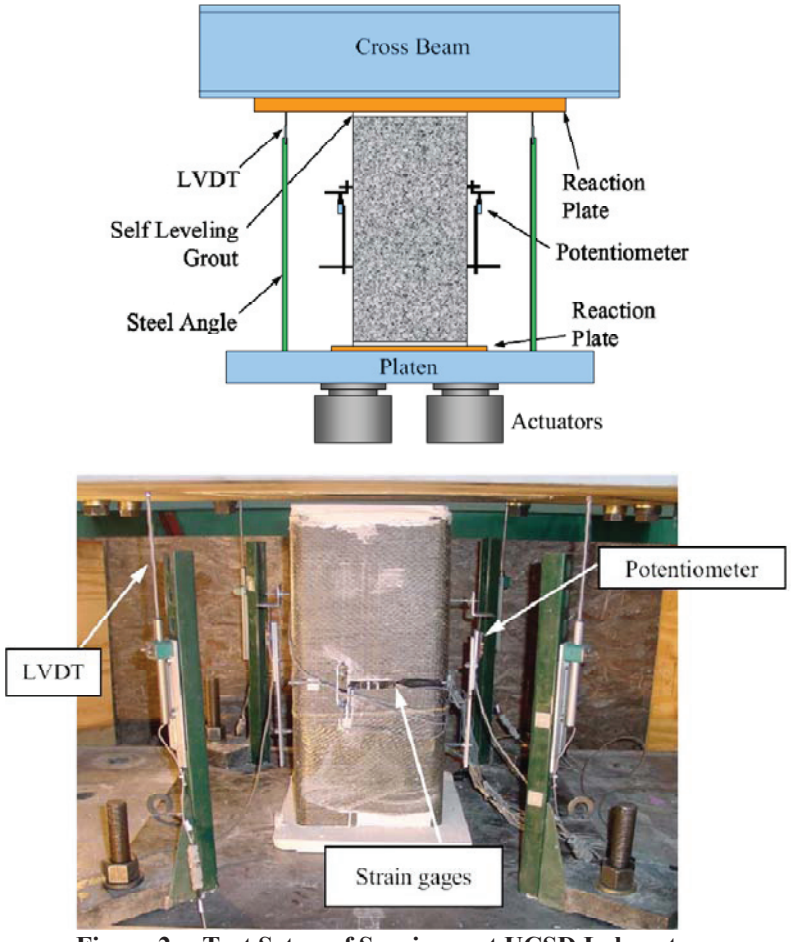

Figure 2 -- Test Setup of Specimen at UCSD Laboratory.

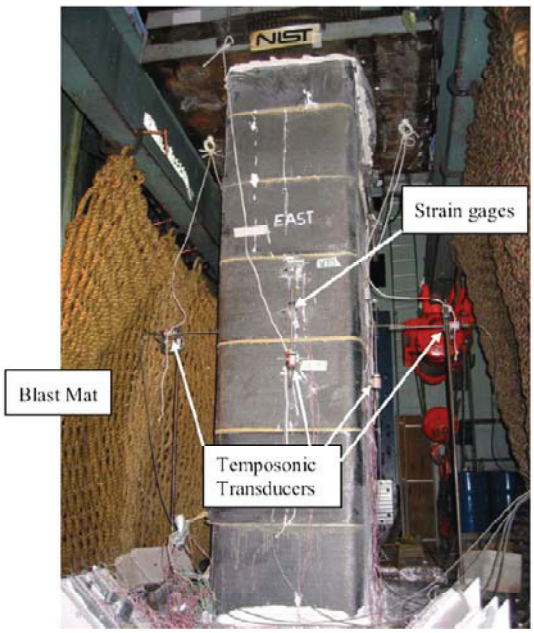

Figure 3 -- Test Setup of Specimen at NIST Laboratory.

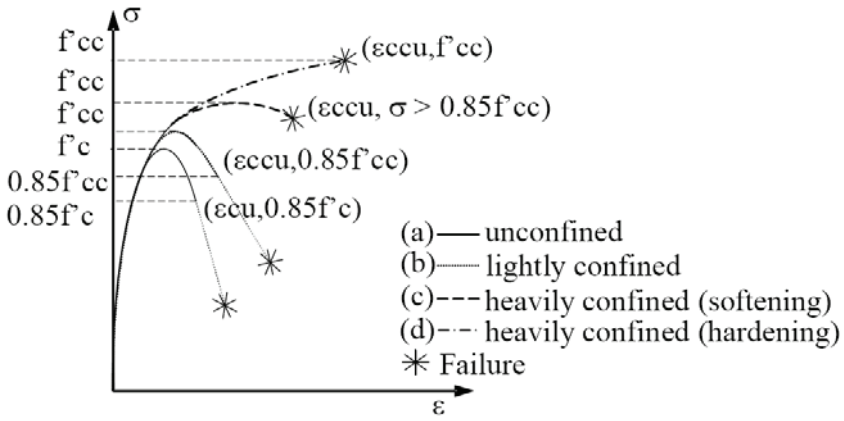

Figure 4 -- Schematic Stress-Strain Behavior of Unconfined and Confined Columns (Rocca et al. 2007).

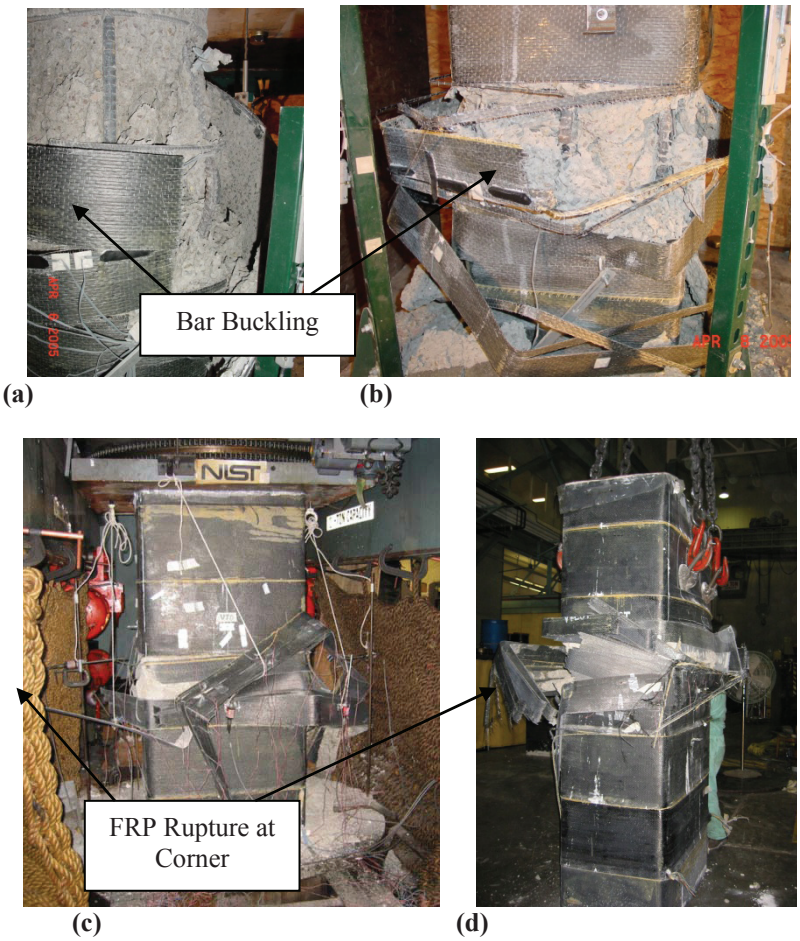

Figure 5 -- FRP-Wrapped RC Columns after Testing: (a) Specimen A2; (b) Specimen C2; (c) Specimen G2; (d) Specimen H2.

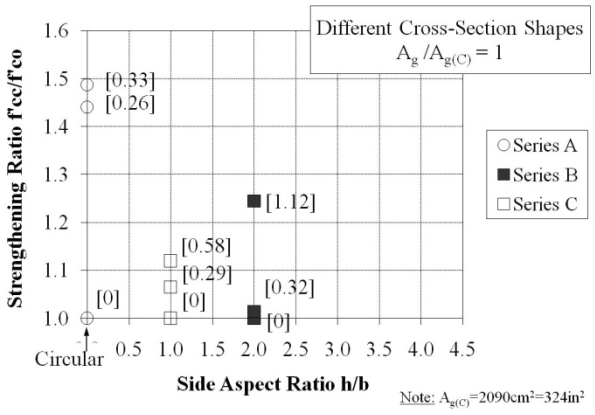

(a)

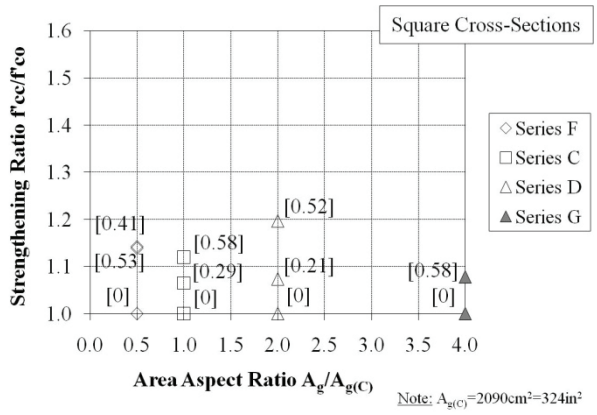

(b)

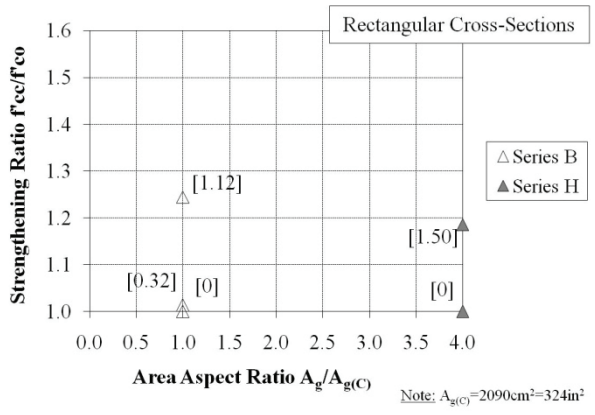

(c)

Figure 6 -- Strengthening Performance of RC Columns in Test Program.

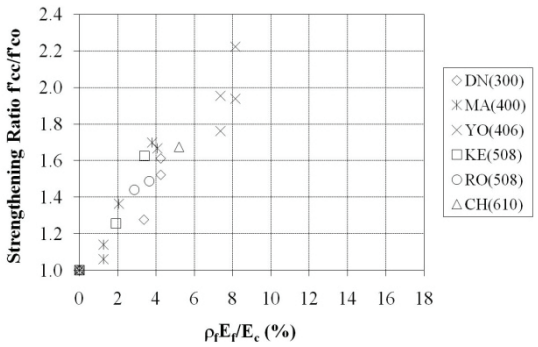

(a) Circular Cross-Sections

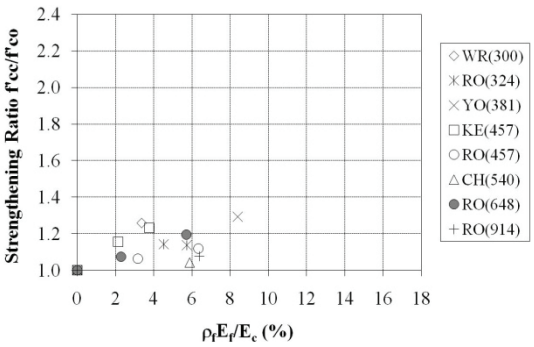

(b) Square Cross-Sections

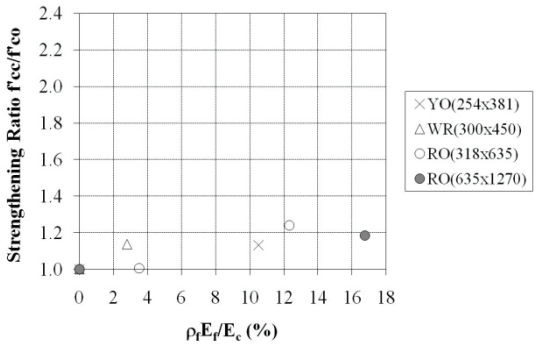

(c) Rectangular Cross-Sections

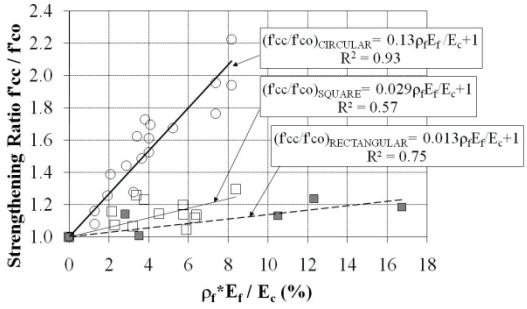

(d) Different Cross-Sections Shapes

Figure 7 -- Global Strengthening Performance of FRP-Confined RC Columns.

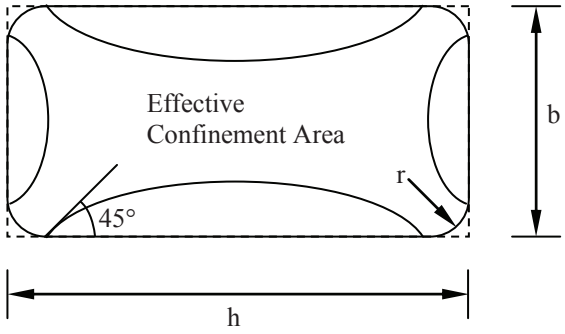

Figure 8 – Effectively Confined Concrete in a Non-Circular Cross-Section.

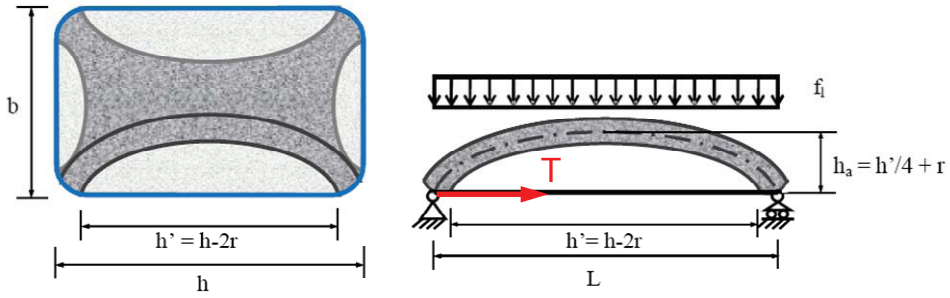

Figure 9 – Schematic of Idealization of Confined Concrete Portion.

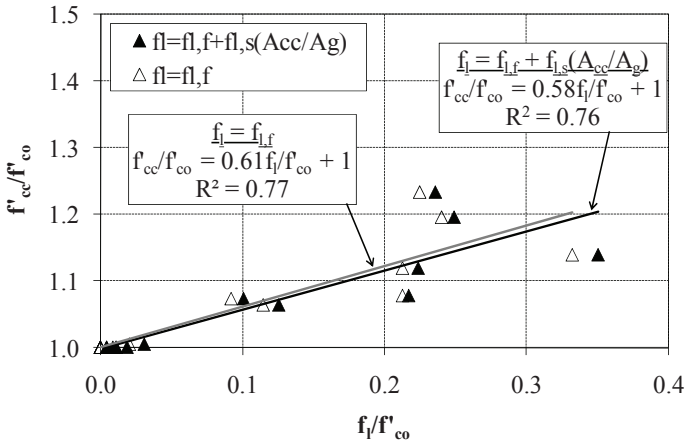

Figure 10 – Determination of Efficiency Factor "k".

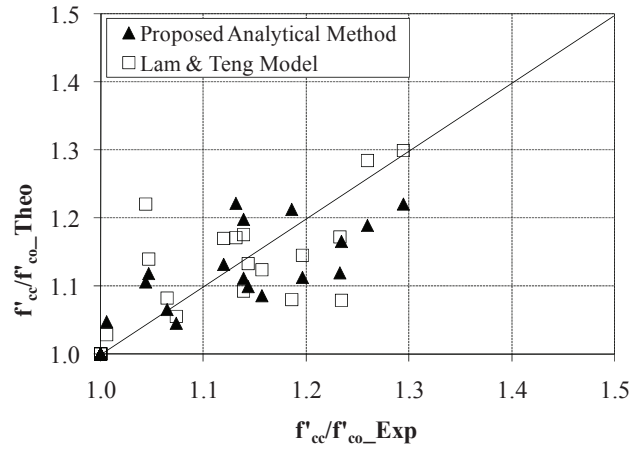

Figure 11 -- Theoretical vs. Experimental Comparison of f'_{cc}/f'_{co}.